# Atomistic structures of nano-engineered SiC and radiation-induced amorphization resistance

Kenta Imada,[1] Manabu Ishimaru,[1,*] Kazuhisa Sato,[2] Haizhou Xue,[3] Yanwen Zhang,[4,3] Steven Shannon[5], William J. Weber,[3,4]

[1]*Department of Materials Science and Engineering, Kyushu Institute of Technology, Kitakyushu, Fukuoka 804-8550, Japan*

[2]*Institute for Materials Research, Tohoku University, Sendai, Miyagi 980-8577, Japan*

[3]*Materials Science and Engineering Department, University of Tennessee, Knoxville, TN 37996-2200, USA*

[4]*Materials Science and Technology Division, Oak Ridge National Laboratory, Tennessee 37831-6138, USA*

[5]*Department of Nuclear Engineering, North Carolina State University, Raleigh, North Carolina 27695, USA*

## Abstract

Nano-engineered 3C-SiC thin films, which possess columnar structures with high-density stacking faults and twins, were irradiated with 2 MeV Si ions at cryogenic and room temperatures. From cross-sectional transmission electron microscopy observations in combination with Monte Carlo simulations based on the Stopping and Range of Ions in Matter code, it was found that their amorphization resistance is six times greater than *bulk* crystalline SiC at room temperature. High-angle bright-field images taken by spherical aberration corrected scanning transmission electron microscopy revealed that the distortion of atomic configurations is localized near the stacking faults. The resultant strain field probably contributes to the enhancement of radiation tolerance of this material.

*To whom correspondence should be addressed. E-mail: ishimaru@post.matsc.kyutech.ac.jp

Understanding structural changes of matter under extreme conditions is of technological importance to predict performance and lifetimes of materials and to avoid serious accident. Nuclear materials are often exposed under harsh radiation environments that induce atomic displacement in materials. Long-term operations under such extreme environments lead to damage accumulation, and consequently severe degradation of the mechanical properties of the materials can occur due to volume swelling, amorphization, and concomitant micro-cracking. Currently, substantial effort has been dedicated to develop radiation tolerant materials [1-4]. Introduction of a large amount of interfaces into materials is expected to enhance radiation tolerance, since they act as effective defect sinks. In fact, several experimental and theoretical studies demonstrated that the introduction of grain boundaries, interfaces, and pores is useful to improve radiation resistivity of conventional *bulk* crystalline materials [5-12].

Silicon carbide (SiC) and its composite materials are anticipated as structure materials for next-generation fusion and fission reactors, because of their superior high temperature mechanical properties and inherent low-induced radioactivity [13]. We have recently prepared nano-engineered 3C-SiC (NE-SiC) in which nanolayered planar defects are intentionally introduced, and examined its radiation-induced amorphization resistance by transmission electron microscopy (TEM) [14]. Although *bulk* SiC becomes amorphous at 0.81 dpa under irradiation with 0.58 MeV Si ions at room temperature [15], it has been found that NE-SiC maintains its crystallinity up to 3.5 dpa under 2 MeV Si ion-irradiation at room temperature. Jamison *et al.* [16] examined structural changes of NE-SiC under electron-beam irradiation using *in situ* TEM. As a consequence, they found that damage threshold for amorphization is five times higher than single crystalline SiC. In contrast, it was reported that NE-SiC exhibits a lower radiation resistance than microcrystalline SiC under *in situ* TEM irradiation with 1 MeV Kr ions at temperatures ranging from 300 K to 450 K [17]. This

means that the radiation response of NE-SiC remains an open question. In the present study, we examined amorphization resistance of NE-SiC irradiated with Si ions at cryogenic temperature. In addition, spherical aberration ($C_S$) corrected microscopy was utilized to identify atomistic structures of planar defects in NE-SiC which probably have an impact on point defects migration and concomitant damage recovery processes.

The SiC thin films grown on a Si (001) wafer were prepared by low-pressure chemical vapour deposition utilizing dual precursor feed gases. The primary feed gases are dichlorosilane ($H_2SiCl_2$), acetylene ($C_2H_2$), and ammonia ($NH_3$). The initial step involves a carbonization stage, in which an ultra-thin carbon film is deposited on the Si substrate, to facilitate proper film quality and to promote stoichiometry. The process temperature is 900 $^oC$. The details of the sample preparation techniques were described elsewhere [14]. The as-deposited specimens were irradiated with 2 MeV Si ions at 165 K and room temperature. The calibration of energy and ion fluence was reported previously [18]. The specimens were characterized by TEM and scanning transmission electron microscopy (STEM). Conventional cross-sectional TEM observations were performed using a JEOL JEM-4000FX (operated at 400 kV) and a JEM-3000F (300 kV). Atomistic structures of planar defects were characterized by a JEM-ARM200F (200 kV), equipped with a $C_S$ corrector for a probe forming system and a cold field emission gun.

As we reported previously, as-deposited 3C-SiC thin films possess a columnar structure with the (111) preferential orientation and contain high-density (111) planar defects, such as stacking faults and twins, nearly perpendicular to the growth direction [14,19]. Figure 1(a) shows a cross-sectional bright-field (BF) TEM image of NE-SiC/Si substrate irradiated with 2 MeV Si ions to a fluence of $5x10^{15}$ $cm^{-2}$ at 165 K. The uncertainty in the ion fluence is below 10% [18]. The specimen shows uniform contrast except for the contrast due to the thickness difference of the TEM specimen. It should be noted that diffraction contrast due to

crystallites can be seen near the surface. In fact, Bragg spots together with halo rings are observed in the electron diffraction pattern obtained from the SiC thin film (Fig. 1(b)). The intensity maxima in Fig. 1(b) exist along the growth direction, indicating that the (111) preferential orientation is maintained after irradiation. On the other hand, the Si substrate is completely amorphized (Fig. 1(c)). According to a previous study [20], the amorphization dose of Si irradiated with 1 MeV Si ions at liquid nitrogen temperature is $2x10^{14}$ $cm^{-2}$, corresponding to 0.3 dpa (the displacement energy is set to 13 eV for the SRIM calculation). The damage at the SiC/Si interface (0.65 dpa) is beyond this value, and therefore the present result is reasonable. We confirmed that complete amorphization of NE-SiC occurs at a fluence of $10^{16}$ $cm^{-2}$ (not shown).

Figure 1(d) shows a high-resolution TEM image obtained from the center of SiC thin film. Although no remarkable diffraction contrast is observed in the BF-TEM image of Fig. 1(a), nanocrystallites, some of them are surrounded by circles, are evident in the high-resolution TEM image. To determine the interface between the crystalline and amorphous regions in SiC thin film, dark-field TEM observations were performed. Figure 2(a) shows a dark-filed TEM image of the specimen irradiated at cryogenic temperature. For comparison, the result of room temperature irradiated specimen is also shown in Fig. 2(b). It is apparent that nanocolumnar structures are maintained after irradiation in both the specimens, and amorphous/crystalline interface is clearly seen. The graphs overlapped on the dark-field images are damage distributions estimated by Monte Carlo simulations based on Stopping and Range of Ions in Matter (SRIM) code [21]. The displacement energy is assumed to 35 eV for Si and 20 eV for C [22]. The SRIM result reveals that the amorphization of NE-SiC occurs at 0.53 and 3.4 dpa (displacement per target atom) at cryogenic and room temperature irradiations, respectively. According to previous studies, *bulk* SiC irradiated with high-energy Si ions becomes amorphous at ~0.14 (~0.2) dpa at 150 (190) K [23,24] and 0.81

dpa at room temperature [15]. However, the dose for amorphization in *bulk* SiC is very dependent on the local ratio of the electronic to nuclear energy deposition, and the relationship between the amorphization dose and this ratio has been established for *bulk* SiC at 100 K [25] and 300 K [26]. Based on these relationships, the amorphization dose for 2 MeV Si at equivalent depths is 0.41 dpa at 100 K and 0.53 dpa at 300 K. Thus, the amorphization dose for NE-SiC at cryogenic temperature is only slightly higher than that expected in *bulk* SiC under similar irradiation conditions, which is expected due to the immobility of point defects at these temperatures. However, the NE-SiC is six times more radiation resistance than *bulk* SiC at 300 K.

We have recently examined amorphization processes of NE-SiC under electron-beam irradiation using *in situ* TEM and found that radiation-induced point defects, such as interstitials and vacancies, migrate two-dimensionally between the (111) planar defects [19]. The mobility of interstitials and vacancies and defect annihilation rate are probably affected by atomistic structures of planar defects. The development of $C_S$ corrector in electron microscope enables us to observe materials in sub-angstrom spatial resolution [27]. Figure 3(a) shows a $C_S$-corrected BF-STEM image of single crystalline 3C-SiC epitaxially grown on a Si substrate, viewed along the [110] direction of 3C-SiC. The image was obtained by 200 keV incident convergent beams with 20 mrad semiangle. The BF detector collection angles were set to 0-34 mrad, corresponding to high-angle BF (HABF) imaging conditions. To reduce noise, fast Fourier transform filtering was applied using the Gatan DigitalMicrograph software. The large and small dark dots in Fig. 3(a) correspond to Si and C atoms, respectively (*cf.* the simulated image shown as an inset). The atomic distance of Si-C bilayer is 0.109 nm in the [110] projection of 3C-SiC (lattice parameter: $a$=0.436 nm), and they are clearly separated by $C_S$-corrected HABF-STEM. As a consequence, six membered rings are observed. Figure 3(b) shows a HABF-STEM image of the NE-SiC, taken by the

same imaging conditions as Fig. 3(a). In addition to the atomic configuration of 3C-SiC, it is apparent that stacking faults, indicated by lines, exist in NE-SiC: the schematic atomic configuration of 3C-SiC is overlapped on the experimental atomic locations in the right side of the line, while the shift of atomic positions due to the stacking fault is observed in the left side.

Figure 4 shows magnified pictures surrounded with (a) solid and (d) dashed squares in Fig. 3(b), and the corresponding schematic atomic configurations are overlapped on Figs. 4(b) and 4(e). It should be noted that the intensity difference and contrast inversion (surrounded by circles) exist in Figs. 4(a) and 4(d). The HABF-STEM image is the projection of atomic configuration, and the contrast changes suggest the existence of anti-site defects where Si occupies C sub-lattice site, and vice versa. The main purpose is to show the atomic distortion, and therefore the site occupancies of Si and C along the [110] projection are not considered in Figs. 4(b) and 4(e). The HABF-STEM image taken from the region away from the stacking fault is almost the same atomic configuration as Fig. 3(a), and only slight distortion of six membered rings is observed in Fig. 4(c). On the other hand, it is apparent that the atomic configurations at the planar defects are highly distorted (Fig. 4(f)). This suggests that the strain filed is localized around the stacking faults.

On the basis of molecular-dynamics simulations, Wang *et al.* examined the effects of grain boundaries in graphene, where five, seven, and eight membered rings are formed, on damage recovery processes [28]. As a consequence, they found that recombination of vacancies and interstitials can occur locally at grain boundaries due to an inhomogeneous strain field, which serve as effective sinks, resulting in efficient annealing of defects. The atomic configurations in NE-SiC are highly distorted near the stacking faults (Fig. 4), and it is anticipated that the mobility of the point defects are affected by their strain field. In fact, two-dimensional defect diffusion was confirmed in electron-beam irradiated NE-SiC by *in*

*situ* TEM observations [19].

Only six membered rings consisting of heteropolar Si-C bonds are drawn in Fig. 4 as an average structure, but there is a possibility that five, seven, and eight membered rings exist in highly distorted atomic configuration of NE-SiC, like the defects in graphene [28]. Such atomic configurations are unstable, and therefore they appear to be rearranged to six membered rings by trapping vacancies and interstitials, resulting in the self-healing. We propose that the strain field associated with atomic distortion near stacking faults plays an important role for enhancing the radiation resistivity of NE-SiC.

As described earlier, NE-SiC shows greater radiation tolerance than *bulk* SiC under Si ions [14] and electron-beam irradiations [16], as well as under the present study, whereas no improvement was observed in Kr ion-irradiated NE-SiC at elevated temperatures [17]. Irradiation with electrons and light ions mostly generate point defects; whereas, heavy-ion irradiation produces collision cascades that can disrupt the nanostructures, which may decrease the effective radiation tolerance in NE-SC. Clearly, more work is needed to understand these discrepancies.

In conclusion, we examined radiation tolerance of NE-SiC at cryogenic and room temperatures. It was found that NE-SiC is six times more radiation resistant than *bulk* crystalline SiC at room temperature. Advanced electron microscopy techniques based on $C_S$-corrected STEM revealed that the atomic configurations are highly distorted near the stacking faults. The distortion leads to an inhomogeneous strain field, where vacancies and interstitials are preferentially trapped. This is attributed to the enhancement of radiation tolerance in NE-SiC.

This work was supported in part by Grant-in-Aid for Scientific Research (B) (Grant No. 25289249) from the Ministry of Education, Sports, Science, and Technology, Japan (MI), by

the U.S. Department of Energy, Office of Sciences, Basic Energy Sciences, Materials Sciences and Engineering Division (YZ and WJW), and Nuclear Energy University Programs (HX and SS). TEM observations were performed under the Cooperative Research Program of "Network Joint Research Center for Materials and Devices" of ISIR, Osaka University, and under the inter-university cooperative research program of the IMR, Tohoku University.

**References**


[1] W. J. Weber, R. C. Ewing, C. R. A. Catlow, T. Diaz de la Rubia, L. W. Hobbs, C. Kinoshita, Hj. Matzke, A. T. Motta, M. Nastasi, E. K. H. Salje, E. R. Vance, and S. J. Zinkle, J. Mater. Res. **13**, 1434 (1998).

[2] K. E. Sickafus, L. Minervini, R. W. Grimes, J. A. Valdez, M. Ishimaru, F. Li, K. J. McClellan, and T. E. Hartmann, Science **289**, 748 (2000).

[3] K. E. Sickafus, R. W. Grimes, J. A. Valdez, A. Cleave, M. Tang, M. Ishimaru, S. M. Corish, C. R. Stanek, and B. P. Uberuaga, Nature Mater. **6**, 217 (2007).

[4] R. C. Ewing, W. J. Weber, and J. Lian, J. Appl. Phys. **95**, 5949 (2004).

[5] M. Rose, A. G. Balogh, and H. Hahn, Nucl. Instrum. Meth. Phys. Res. B **127/128**, 119 (1997).

[6] Y. Chimi, A. Iwase, N. Ishikawa, M. Kobiyama, T. Inami, and S. Okuda, J. Nucl. Mater. **297**, 355 (2001).

[7] N. Nita, R. Schaeublin, and M. Victoria, J. Nucl. Mater. **329-333**, 953 (2004).

[8] A. Misra, M. J. Demkowicz, X. Zhang, R. G. Hoagland, JOM **59**, 62 (2007).

[9] T. D. Shen, S. Feng, M. Tang, J. A. Valdez, Y.-Q. Wang, and K. E. Sickafus, Appl. Phys. Lett. **90**, 263115 (2007).

[10] E. M. Bringa, J. D. Monk, A. Caro, A. Misra, L. Zepeda-Ruiz, M. Duchaineau, F. Abraham, M. Nastasi, S. T. Picraux, Y. Q. Wang, and D. Farkas, Nano Lett. **12**, 3351 (2012).

[11] R. W. Grimes, R. J. M. Konings, and L. Edwards, Nature Mater. **7**, 683 (2008).

[12] X.-M. Bai, A. F. Voter, R. G. Hoagland, M. Nastasi, and B. P. Uberuaga, Science **327**, 1631 (2010).

[13] Y. Katoh, L. L. Snead, I. Szlufarska, W. J. Weber, Curr. Opin. Solids State Mater. Sci. **16**, 143 (2012).

[14] Y. Zhang, M. Ishimaru, T. Varga, T. Oda, C. Hardiman, H. Xue, Y. Katoh, S. Shannon, and W. J. Weber, Phys. Chem. Chem. Phys. **14**, 13429 (2012).

[15] W. J. Weber, L. M. Wang, N. Yu, and N. J. Hess, Mater. Sci. Eng. A **253**, 62 (1998).

[16] L. Jamison, M.-J. Zheng, S. Shannon, T. Allen, D. Morgan, and I. Szlufarska, J. Nucl. Mater. **445**, 181 (2014).

[17] L. Jamison, K. Sridharan, S. Shannon, and I. Szlufarska, J. Mater. Res. **29**, 2871 (2014).

[18] Y. Zhang, M. L. Crespillo, H. Xue, K. Jin, C.-H. Chen, C. L. Fontana, J. T. Graham, and W. J. Weber, Nucl. Instrum. Meth. Phys. Res. B **338**, 19 (2014).

[19] M. Ishimaru, Y. Zhang, S. Shannon, and W. J. Weber, Appl. Phys. Lett. **103**, 033104 (2013).

[20] J. M. Poate, S. Coffa, D. C. Jacobson, A. Polman, J. A. Roth, G. L. Olson, S. Roorda, W. Sinke, J. S. Custer, M. O. Thompson, F. Spaepen, and E. Donovan, Nucl. Instrum. Meth. Phys. Res. B **55**, 533 (1991).

[21] J. F. Ziegler, SRIM-2008, v. 2008.40, http://www.srim.org.

[22] Y. Zhang, W. J. Weber, W. Jiang, C. M. Wang, V. Shutthanandan, and A. Hallén, J. Appl. Phys. **95**, 4012 (2004).

[23] W. J. Weber, F. Gao, R. Devanathan, W. Jiang, and C. M. Wang, Nucl. Instrum. Meth. Phys. Res. B **216**, 25 (2004).

[24] The same amorphization damage was observed in 1.1 MeV Al ion-irradiated 4H- and 6H-SiC at 150 K: Y. Zhang, W. J. Weber, W. Jiang, A. Hallén, and G. Possnert, J. Appl. Phys. **91**, 6388 (2002).

[25] W. J. Weber, L. Wang, Y. Zhang, W. Jiang, and I.-T. Bae, Nucl. Instrum. Meth. Phys. Res. B **266**, 2793 (2008).

[26] W. J. Weber, Y. Zhang, and L. M. Wang, Nucl. Instrum. Meth. Phys. Res. B **277**, 1 (2012).

[27] Y. R. Lin, C. Y. Ho, C. Y. Hsieh, M. T. Chang, S. C. Lo, F. R. Chen, and J. J. Kai, Appl. Phys. Lett. **104**, 121909 (2014).

[28] B. Wang, Y. Puzyrev, and S. T. Pantelides, Carbon **49**, 3983 (2011).

**Figure captions**

Figure 1. (a) Cross-sectional bright-field image of NE-SiC irradiated with 2 MeV Si ions to a fluence of $5x10^{15}$ $cm^{-2}$ at cryogenic temperature. Electron diffraction patterns taken from (a) SiC thin film and (b) Si substrate. (d) High-resolution TEM image obtained around the center of SiC thin film. Some of the crystallites in amorphous matrix are surrounded by circles.

Figure 2. Cross-sectional dark-field TEM images of NE-SiC irradiated at (a) 165 K and (b) room temperature. The graph overlapped on the images is radiation-induced damage distribution calculated using the SRIM code.

Figure 3. $C_S$-corrected HABF-STEM images of (a) single crystalline SiC and (b) NE-SiC, viewed along the [110] direction. The simulated HABF-STEM image is shown in (a) as an inset. The following parameters were used for the calculation: accelerate voltage of 200 kV, incident convergent beams with 23 mrad semiangle, 1 μm $C_S$ coefficient, and specimen thickness of 20 nm. The BF detector collection angles were set to 0-34 mrad. In (b), stacking faults are indicated by lines.

Figure 4. (a,d) Magnified images of atomic configurations surrounded by (a) solid and (b) dashed lines in Fig. 3(b). Schematic atomic configurations (b,e) with and (c,f) without the images. Large and small circles denote Si and C atoms, respectively.

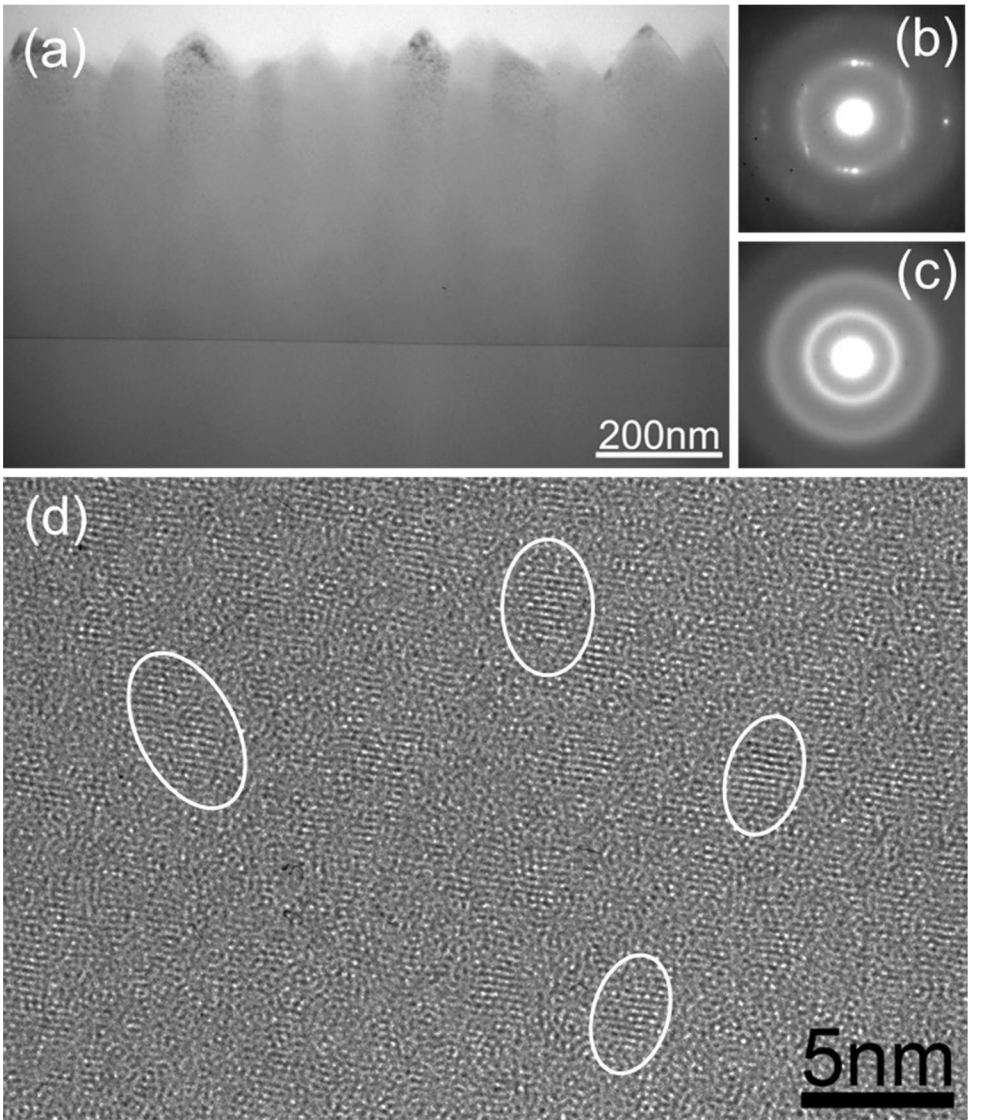
(a)
200nm
(b)
(c)
(d)
5nm

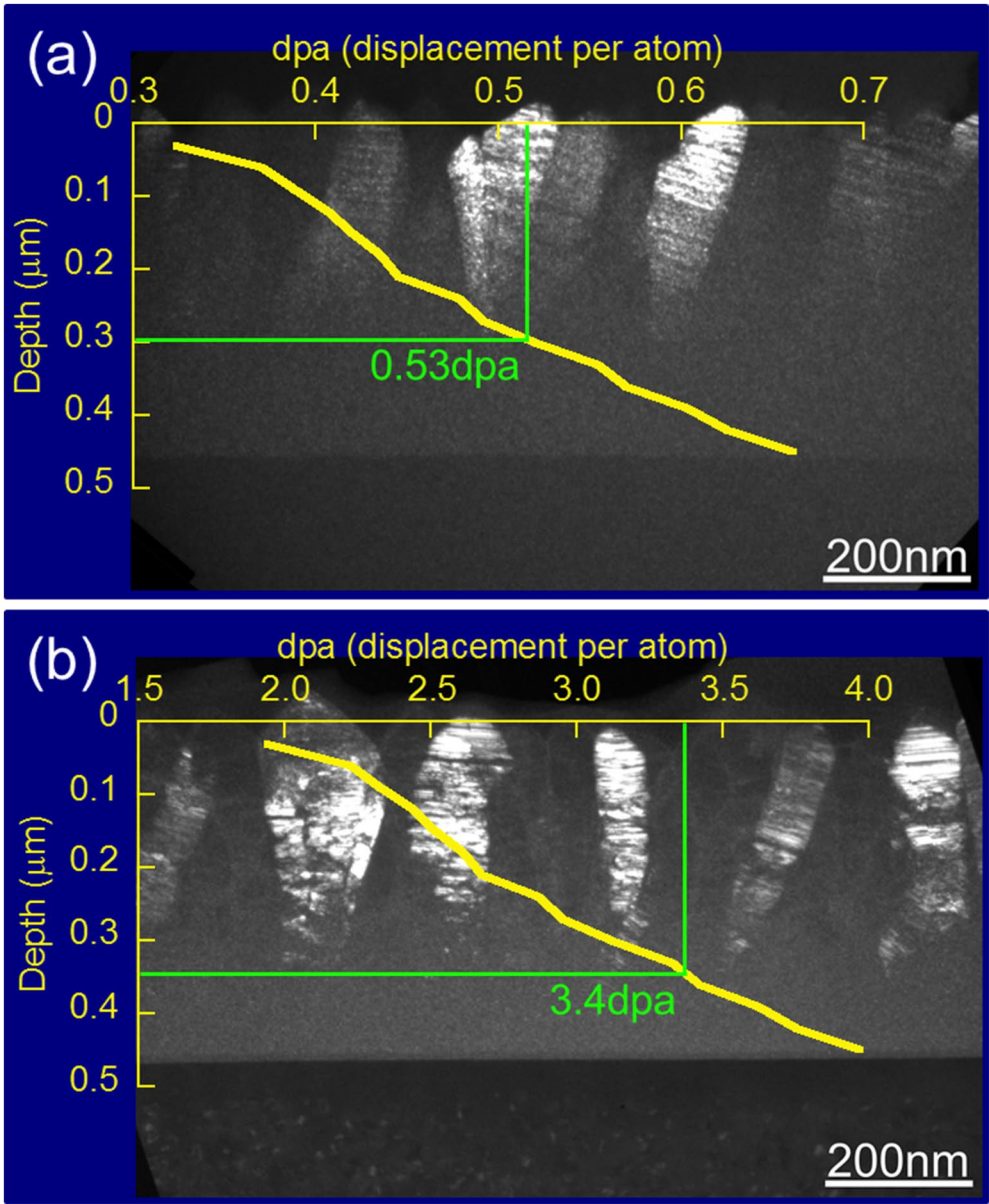
(a)
dpa (displacement per atom)
0.3
0.4
0.5
0.6
0.7
0
0.1
0.2
0.3
0.4
0.5
Depth (μm)
0.53dpa
200nm
(b)
dpa (displacement per atom)
1.5
2.0
2.5
3.0
3.5
4.0
0
0.1
0.2
0.3
0.4
0.5
Depth (μm)
3.4dpa
200nm

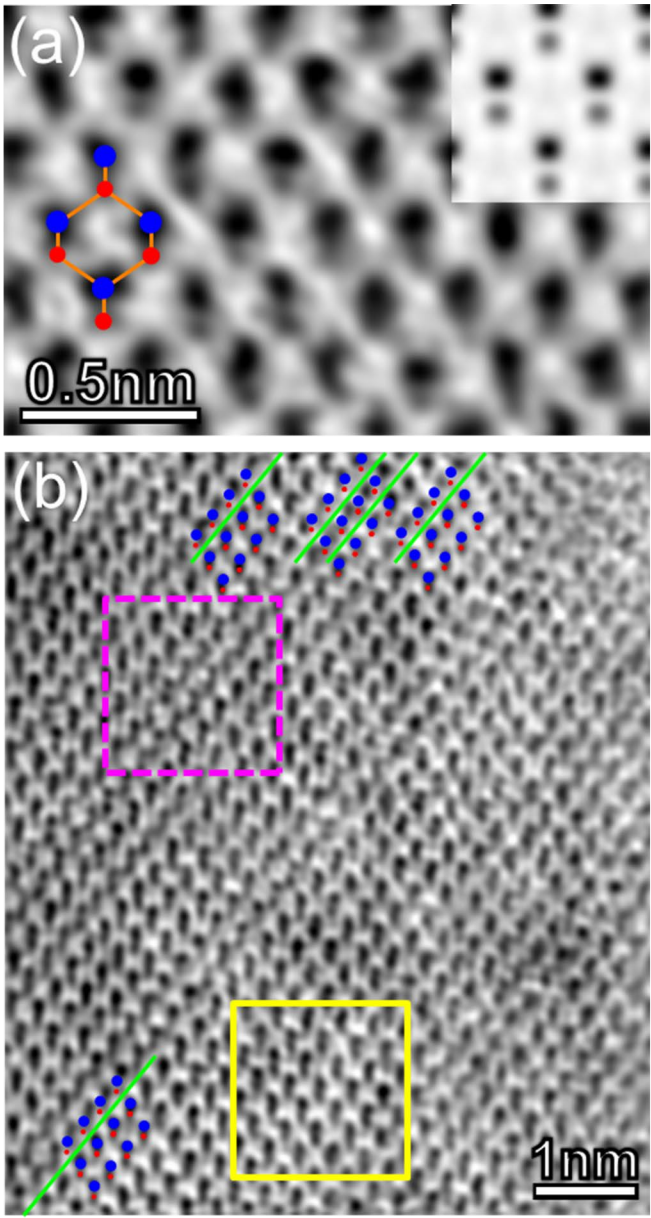
(a)
0.5nm
(b)
1nm

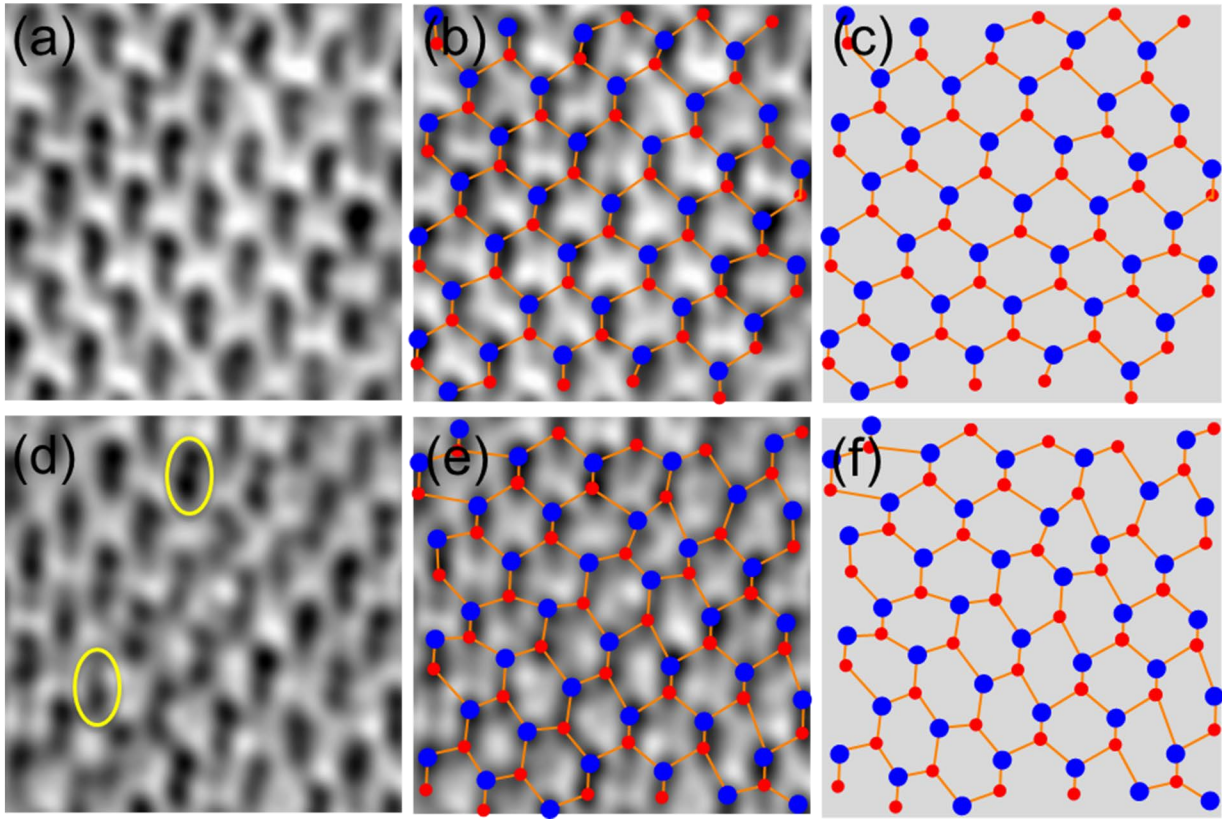
(a)
(b)
(c)
(d)
(e)
(f)